Test Bench - Amplified Piezoelectric Actuator

Dehaeze Thomas

April 3, 2024

Contents

In this chapter, the goal is to make sure that the received APA300ML (shown in Figure 1) are complying with the requirements and that dynamical models of the actuator are well representing its dynamics.

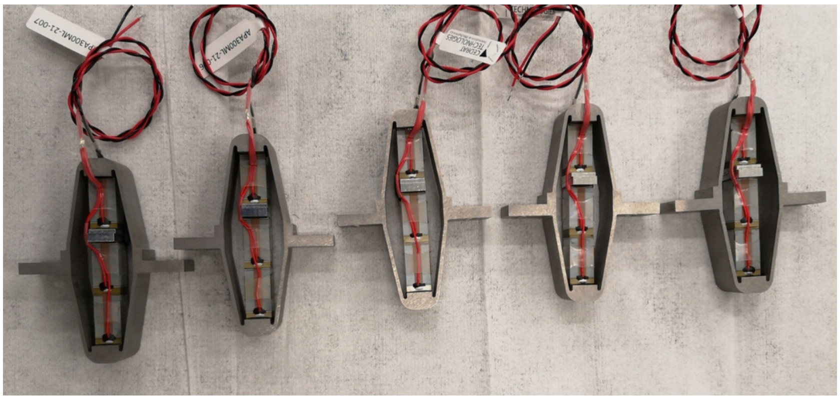

Figure 1: Picture of 5 out of the 7 received APA300ML

In section 1, the mechanical tolerances of the APA300ML interfaces are checked together with the electrical properties of the piezoelectric stacks, the achievable stroke. Flexible modes of the APA300ML are computed with a finite element model and compared with measurements.

Using a dedicated test bench, dynamical measurements are performed (Section 2). The dynamics from the generated DAC voltage (going through the voltage amplifier and then to two actuator stacks) to the induced axial displacement and to the measured voltage across the force sensor stack are estimated. Integral Force Feedback is experimentally applied and the damped plants are estimated for several feedback gains.

Two different models of the APA300ML are then presented. First, in Section 3, a two degrees of freedom model is presented, tuned and compared with the measured dynamics. This model is proven to accurately simulate the APA300ML's axial dynamics.

Then, in Section 4, a *super element* of the APA300ML is extracted using a finite element model and imported in Simscape. This more complex model is also shown to well capture the axial dynamics of the APA300ML.

Sections	**Matlab File**
Section 1	`test_apa_1_basic_meas.m`
Section 2	`test_apa_2_dynamics.m`
Section 3	`test_apa_3_model_2dof.m`
Section 4	`test_apa_4_model_flexible.m`

Table 1: Report sections and corresponding Matlab files

1 First Basic Measurements

Before measuring the dynamical characteristics of the APA300ML, first simple measurements are performed. First, the tolerances (especially flatness) of the mechanical interfaces are checked in Section 1.1. Then, the capacitance of the piezoelectric stacks is measured in Section 1.2. The achievable stroke of the APA300ML is measured using a displacement probe in Section 1.3. Finally, in Section 1.4, the flexible modes of the APA are measured and compared with a finite element model.

1.1 Geometrical Measurements

To measure the flatness of the two mechanical interfaces of the APA300ML, a small measurement bench is installed on top of a metrology granite with excellent flatness. As shown in Figure 1.1, the APA is fixed to a clamp while a measuring probe[1] is used to measure the height of 4 points on each of the APA300ML interfaces. From the X-Y-Z coordinates of the measured 8 points, the flatness is estimated by best fitting[2] a plane through all the points. The measured flatness, summarized in Table 1.1, are within the specifications.

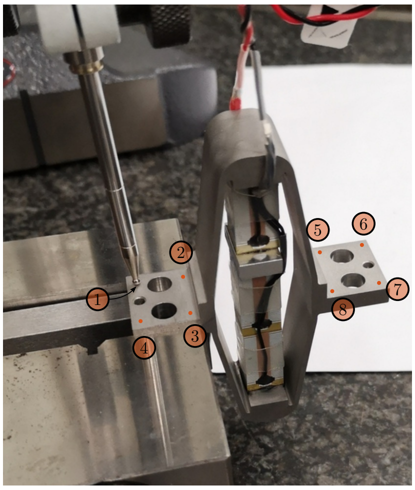

Figure 1.1: Measurement setup for flatness estimation

	Flatness $[\mu m]$
APA 1	8.9
APA 2	3.1
APA 3	9.1
APA 4	3.0
APA 5	1.9
APA 6	7.1
APA 7	18.7

Table 1.1: Estimated flatness of the APA300ML interfaces

[1] Heidenhain MT25, specified accuracy of $\pm 0.5\,\mu m$
[2] The Matlab `fminsearch` command is used to fit the plane

1.2 Electrical Measurements

From the documentation of the APA300ML, the total capacitance of the three stacks should be between $18\,\mu F$ and $26\,\mu F$ with a nominal capacitance of $20\,\mu F$.

The piezoelectric stacks capacitance of the APA300ML have been measured with the LCR meter[3] shown in Figure 1.2. The two stacks used as an actuator and the stack used as a force sensor are measured separately. The measured capacitance are summarized in Table 1.2 and the average capacitance of one stack is $\approx 5 \mu F$. However, the measured capacitance of the stacks of "APA 3" is only half of the expected capacitance. This may indicate a manufacturing defect.

The measured capacitance is found to be lower than the specified one. This may be due to the fact that the manufacturer measures the capacitance with large signals ($-20\,V$ to $150\,V$) while it was here measured with small signals [1].

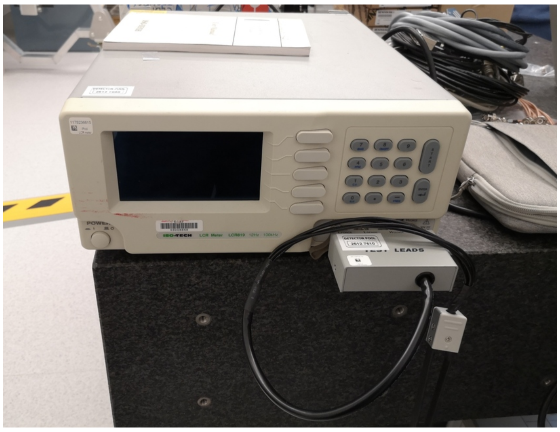

Figure 1.2: Used LCR meter

	Sensor Stack	Actuator Stacks
APA 1	5.10	10.03
APA 2	4.99	9.85
APA 3	1.72	5.18
APA 4	4.94	9.82
APA 5	4.90	9.66
APA 6	4.99	9.91
APA 7	4.85	9.85

Table 1.2: Measured capacitance in μF

1.3 Stroke and Hysteresis Measurement

In order to verify that the stroke of the APA300ML is as specified in the datasheet, one side of the APA is fixed to the granite, and a displacement probe[4] is located on the other side as shown in Figure 1.3.

Then, the voltage across the two actuator stacks is varied from $-20\,V$ to $150\,V$ using a DAC and a voltage amplifier. Note that the voltage is here slowly varied as the displacement probe has a very low measurement bandwidth (see Figure 1.4a).

The measured APA displacement is shown as a function of the applied voltage in Figure 1.4b. Typical hysteresis curves for piezoelectric stack actuators can be observed. The measured stroke is approximately $250\,\mu m$ when using only two of the three stacks, which is enough for the current application. This is even above what is specified as the nominal stroke in the data-sheet ($304\,\mu m$, therefore $\approx 200\,\mu m$ if only two stacks are used).

[3] LCR-819 from Gwinstek, specified accuracy of 0.05%, measured frequency is set at 1 kHz
[4] Millimar 1318 probe, specified linearity better than $1\,\mu m$

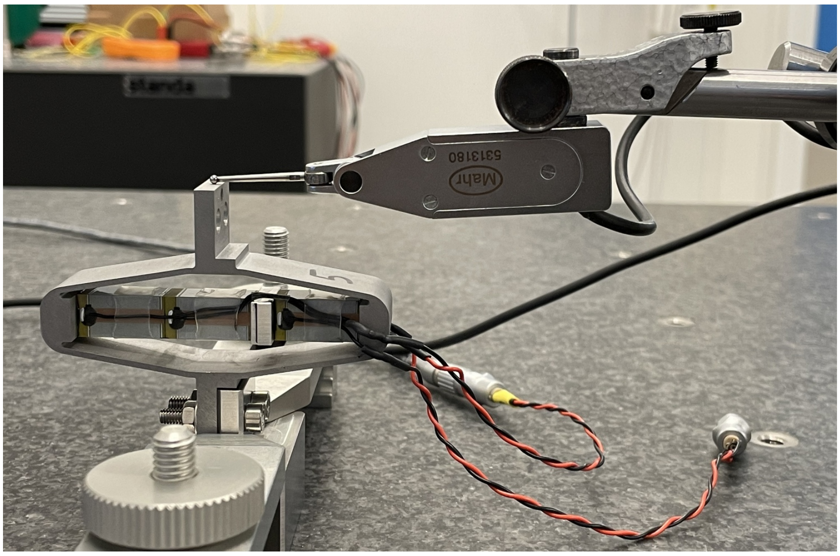

Figure 1.3: Bench to measured the APA stroke

It is clear from Figure 1.4b that "APA 3" has an issue compared to the other units. This confirms the abnormal electrical measurements made in Section 1.2. This unit was send sent back to Cedrat and a new one was shipped back. From now on, only the six APA that behave as expected will be used.

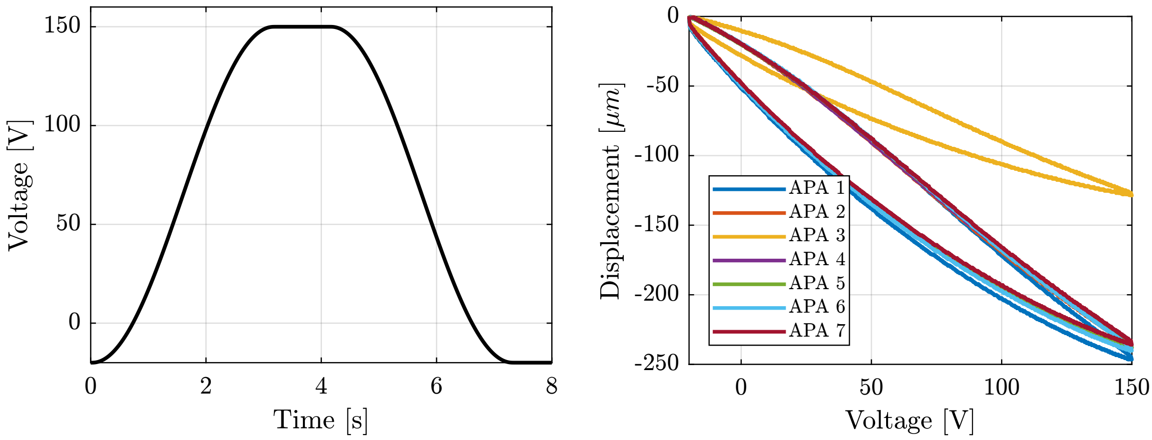

(a) Applied voltage for stroke estimation

(b) Hysteresis curves of the APA

Figure 1.4: Generated voltage across the two piezoelectric stack actuators to estimate the stroke of the APA300ML (a). Measured displacement as a function of the applied voltage (b)

1.4 Flexible Mode Measurement

In this section, the flexible modes of the APA300ML are investigated both experimentally and using a Finite Element Model. To experimentally estimate these modes, the APA is fixed on one end (see Figure 1.6). A Laser Doppler Vibrometer[5] is used to measure the difference of motion between two

[5]Polytec controller 3001 with sensor heads OFV512

"red" points and an instrumented hammer[6] is used to excite the flexible modes. Using this setup, the transfer function from the injected force to the measured rotation can be computed in different conditions and the frequency and mode shapes of the flexible modes can be estimated.

The flexible modes for the same condition (i.e. one mechanical interface of the APA300ML fixed) are estimated using a finite element software and the results are shown in Figure 1.5.

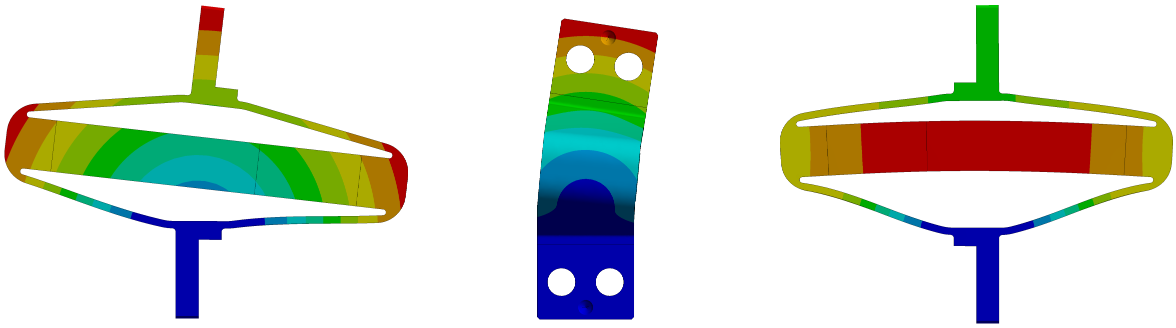

(a) Y-bending mode (268Hz) **(b)** X-bending mode (399Hz) **(c)** Z-axial mode (706Hz)

Figure 1.5: First three modes of the APA300ML in a fix-free condition estimated from a Finite Element Model

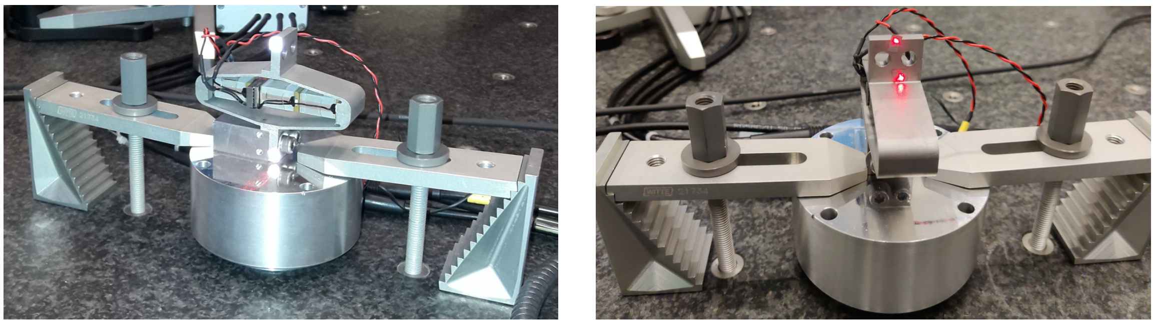

(a) X bending **(b)** Y Bending

Figure 1.6: Experimental setup to measured flexible modes of the APA300ML. For the bending in the X direction (a), the impact point is located at the back of the top measurement point. For the bending in the Y direction (b), the impact point is located on the back surface of the top interface (on the back of the 2 measurements points).

The measured frequency response functions computed from the experimental setups of figures 1.6a and 1.6b are shown in Figure 1.7. The y bending mode is observed at 280 Hz and the x bending mode is at 412 Hz. These modes are measured at higher frequencies than the estimated frequencies from the Finite Element Model (see frequencies in Figure 1.6). This is opposite to what is usually observed (i.e. having lower resonance frequencies in practice than the estimation from a finite element model). This could be explained by underestimation of the Young's modulus of the steel used for the shell (190 GPa was used for the model, but steel with Young's modulus of 210 GPa could have been used). Another explanation is the shape difference between the manufactured APA300ML and the 3D model, for instance thicker blades.

[6] Kistler 9722A

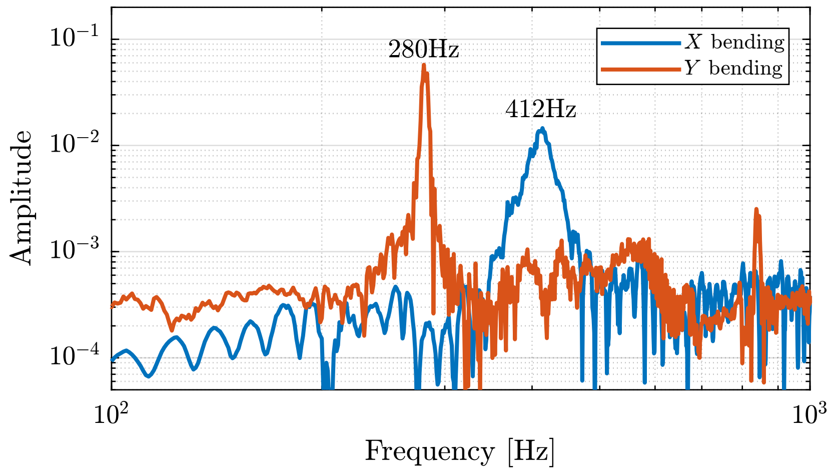

Figure 1.7: Obtained frequency response functions for the 2 tests with the instrumented hammer and the laser vibrometer. The Y-bending mode is measured at 280 Hz and the X-bending mode at 412 Hz

2 Dynamical measurements

After the basic measurements on the APA were performed in Section 1, a new test bench is used to better characterize the dynamics of the APA300ML. This test bench, depicted in Figure 2.1, comprises the APA300ML fixed at one end to a stationary granite block, and at the other end to a 5kg granite block that is vertically guided by an air bearing. That way, there is no friction when actuating the APA300ML, and it will be easier to characterize its behavior independently of other factors. An encoder[1] is utilized to measure the relative movement between the two granite blocks, thereby measuring the axial displacement of the APA.

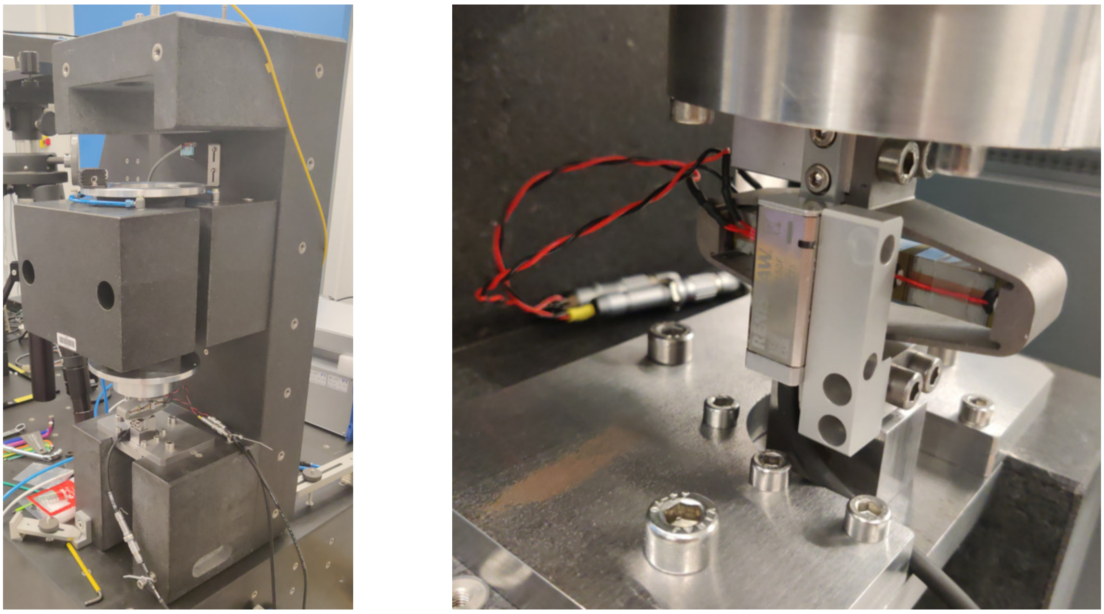

(a) Picture of the test bench **(b)** Zoom on the APA with the encoder

Figure 2.1: Schematic of the test bench used to estimate the dynamics of the APA300ML

The bench is schematically shown in Figure 2.2 with all the associated signals. It will be first used to estimate the hysteresis from the piezoelectric stack (Section 2.1) as well as the axial stiffness of the APA300ML (Section 2.2). Then, the frequency response functions from the DAC voltage u to the displacement d_e and to the voltage V_s are measured in Section 2.3. The presence of a non minimum phase zero found on the transfer function from u to V_s is investigated in Section 2.4. In order to limit the low frequency gain of the transfer function from u to V_s, a resistor is added across the force sensor stack (Section 2.5). Finally, the Integral Force Feedback is implemented, and the amount of damping added is experimentally estimated in Section 2.6.

[1]Renishaw Vionic, resolution of $2.5\,nm$

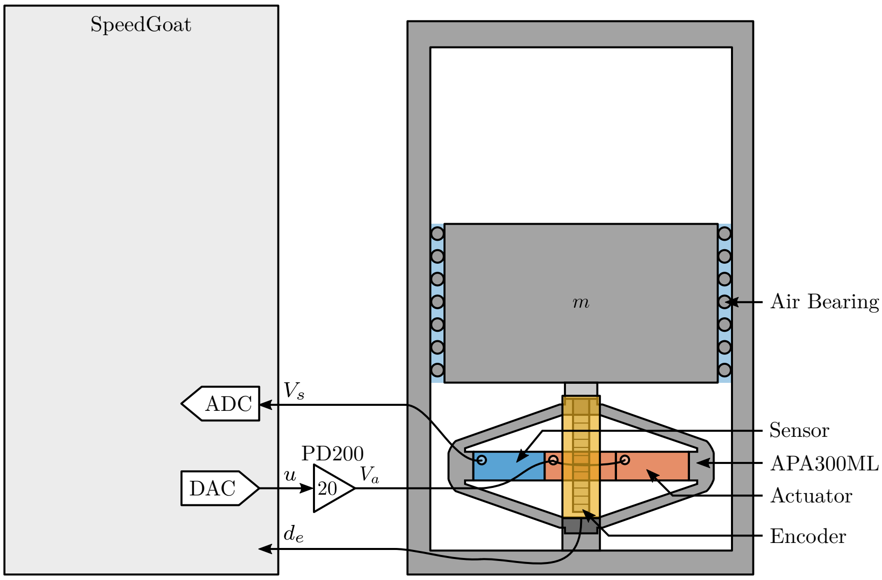

Figure 2.2: Schematic of the Test Bench used to measured the dynamics of the APA300ML. u is the output DAC voltage, V_a the output amplifier voltage (i.e. voltage applied across the actuator stacks), d_e the measured displacement by the encoder and V_s the measured voltage across the sensor stack.

2.1 Hysteresis

As the payload is vertically guided without friction, the hysteresis of the APA can be estimated from the motion of the payload. Do to so, a quasi static[2] sinusoidal excitation V_a with an offset of $65\,V$ (halfway between $-20\,V$ and $150\,V$) and with an amplitude varying from $4\,V$ up to $80\,V$ is generated using the DAC. For each excitation amplitude, the vertical displacement d_e of the mass is measured and displayed as a function of the applied voltage in Figure 2.3. This is the typical behavior expected from a PZT stack actuator where the hysteresis increases as a function of the applied voltage amplitude [2, chap. 1.4].

2.2 Axial stiffness

In order to estimate the stiffness of the APA, a weight with known mass $m_a = 6.4\,\text{kg}$ is added on top of the suspended granite and the deflection d_e is measured using the encoder. The APA stiffness can then be estimated from equation (2.1).

$$k_{\text{apa}} = \frac{m_a g}{\Delta d_e} \tag{2.1}$$

The measured displacement d_e as a function of time is shown in Figure 2.4. It can be seen that there are some drifts in the measured displacement (probably due to piezoelectric creep) and the that displacement does not come back to the initial position after the mass is removed (probably due to piezoelectric hysteresis). These two effects induce some uncertainties in the measured stiffness.

[2]Frequency of the sinusoidal wave is 1 Hz

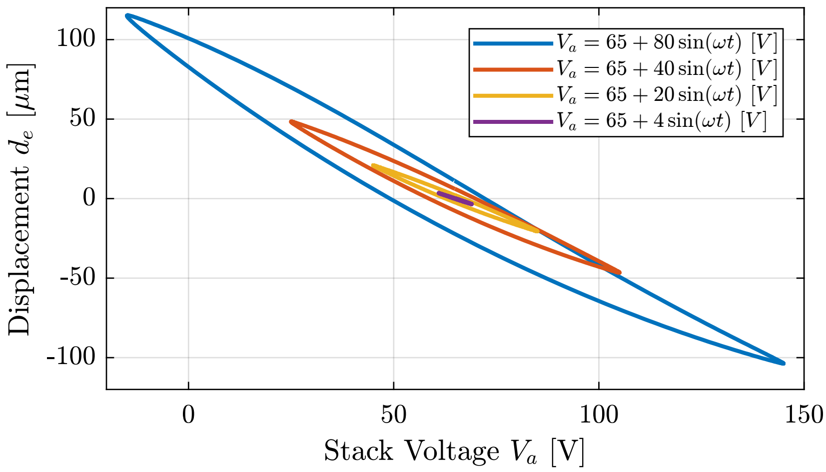

Figure 2.3: Obtained hysteresis curves (displacement as a function of applied voltage) for multiple excitation amplitudes

The stiffnesses are computed for all the APA from the two displacements d_1 and d_2 (see Figure 2.4) leading to two stiffness estimations k_1 and k_2. These estimated stiffnesses are summarized in Table 2.1 and are found to be close to the specified nominal stiffness of the APA300ML $k = 1.8\,N/\mu m$.

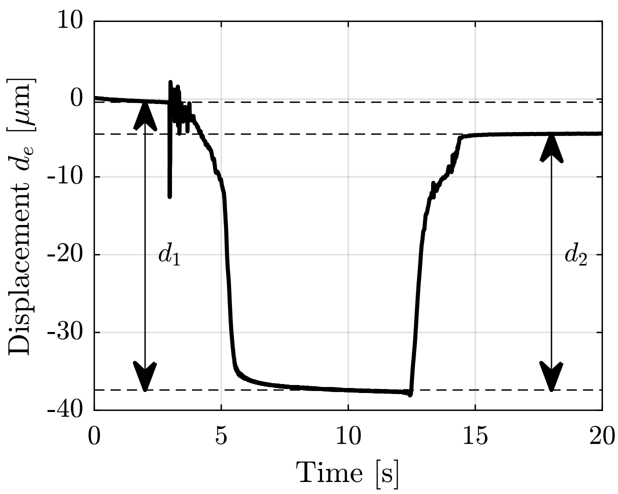

Figure 2.4: Measured displacement when adding (at $t \approx 3\,s$) and removing (at $t \approx 13\,s$) the mass

APA	k_1	k_2
1	1.68	1.9
2	1.69	1.9
4	1.7	1.91
5	1.7	1.93
6	1.7	1.92
8	1.73	1.98

Table 2.1: Measured axial stiffnesses (in $N/\mu m$)

The stiffness can also be computed using equation (2.2) by knowing the main vertical resonance frequency $\omega_z \approx 95\,\text{Hz}$ (estimated by the dynamical measurements shown in section 2.3) and the suspended mass $m_{\text{sus}} = 5.7\,\text{kg}$.

$$\omega_z = \sqrt{\frac{k}{m_{\text{sus}}}} \tag{2.2}$$

The obtain stiffness is $k \approx 2\,N/\mu m$ which is close to the values found in the documentation and by the "static deflection" method.

It is important to note that changes to the electrical impedance connected to the piezoelectric stacks impacts the mechanical compliance (or stiffness) of the piezoelectric stack [3, chap. 2].

To estimate this effect for the APA300ML, its stiffness is estimated using the "static deflection" method in two cases:

- k_{os}: piezoelectric stacks left unconnected (or connect to the high impedance ADC)
- k_{sc}: piezoelectric stacks short circuited (or connected to the voltage amplifier with small output impedance)

It is found that the open-circuit stiffness is estimated at $k_{\text{oc}} \approx 2.3\, N/\mu m$ while the the closed-circuit stiffness $k_{\text{sc}} \approx 1.7\, N/\mu m$.

2.3 Dynamics

In this section, the dynamics from the excitation voltage u to the encoder measured displacement d_e and to the force sensor voltage V_s is identified.

First, the dynamics from u to d_e for the six APA300ML are compared in Figure 2.5a. The obtained frequency response functions are similar to that of a (second order) mass-spring-damper system with:

- A "stiffness line" indicating a static gain equal to $\approx -17\, \mu m/V$. The minus sign comes from the fact that an increase in voltage stretches the piezoelectric stack which reduces the height of the APA
- A lightly damped resonance at 95 Hz
- A "mass line" up to $\approx$ 800 Hz, above which additional resonances appear. These additional resonances might be coming from the limited stiffness of the encoder support or from the limited compliance of the APA support. Flexible modes studied in section 1.4 seems not to impact the measured axial motion of the actuator.

The dynamics from u to the measured voltage across the sensor stack V_s for the six APA300ML are compared in Figure 2.5b.

A lightly damped resonance (pole) is observed at 95 Hz and a lightly damped anti-resonance (zero) at 41 Hz. No additional resonances is present up to at least 2 kHz indicating that Integral Force Feedback can be applied without stability issues from high frequency flexible modes. The zero at 41 Hz seems to be non-minimum phase (the phase *decreases* by 180 degrees whereas it should have *increased* by 180 degrees for a minimum phase zero). This is investigated in Section 2.4.

As illustrated by the Root Locus, the poles of the *closed-loop* system converges to the zeros of the *open-loop* plant as the feedback gain increases. The significance of this behavior varies on the type of sensor used as explained in [4, chap. 7.6]. Considering the transfer function from u to V_s, if a controller with a very high gain is applied such that the sensor stack voltage V_s is kept at zero, the sensor (and by extension, the actuator stacks since they are in series) experiences negligible stress and strain. Consequently, the closed-loop system would virtually corresponds to one where the piezoelectric stacks are absent, leaving only the mechanical shell. From this analysis, it can be inferred that the axial stiffness of the shell is $k_{\text{shell}} = m\omega_0^2 = 5.7 \cdot (2\pi \cdot 41)^2 = 0.38\, N/\mu m$ (which is close to what is found using a finite element model).

All the identified dynamics of the six APA300ML (both when looking at the encoder in Figure 2.5a and at the force sensor in Figure 2.5b) are almost identical, indicating good manufacturing repeatability for the piezoelectric stacks and the mechanical shell.

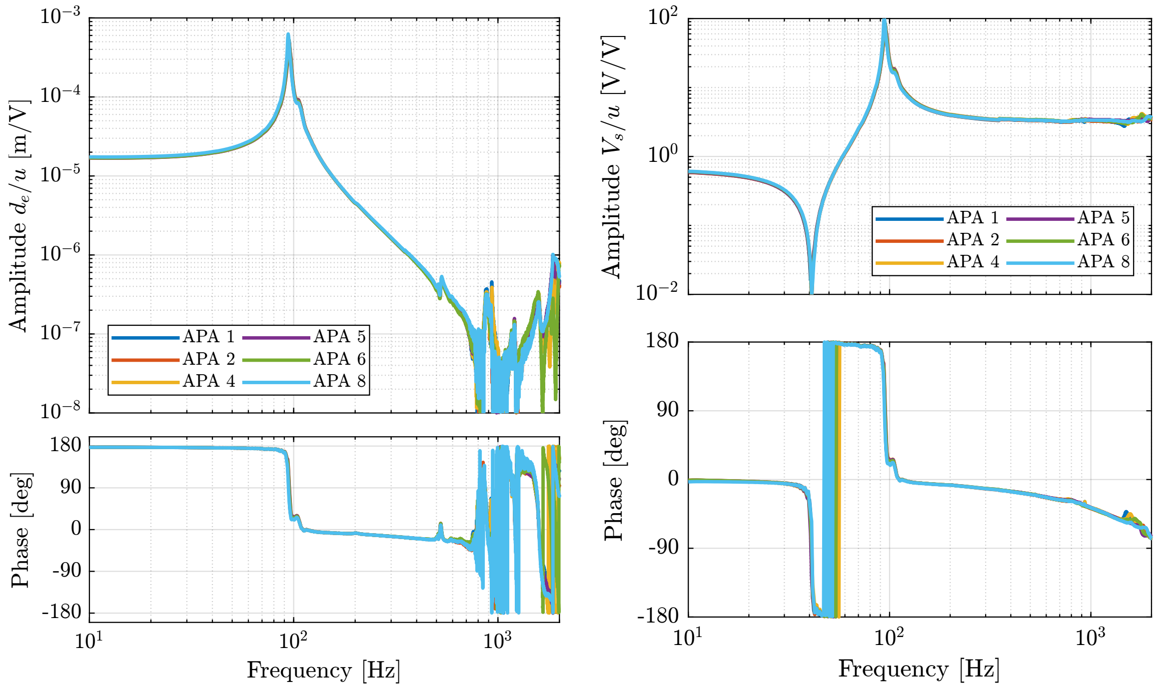

(a) FRF from u to d_e

(b) FRF from u to V_s

Figure 2.5: Measured frequency response function from generated voltage u to the encoder displacement d_e (a) and to the force sensor voltage V_s (b) for the six APA300ML

2.4 Non Minimum Phase Zero?

It was surprising to observe a non-minimum phase behavior for the zero on the transfer function from u to V_s (Figure 2.5b). It was initially thought that this non-minimum phase behavior is an artifact coming from the measurement. A longer measurement was performed with different excitation signals (noise, slow sine sweep, etc.) to see it the phase behavior of the zero changes. Results of one long measurement is shown in Figure 2.6. The coherence (Figure 2.6a) is good even in the vicinity of the lightly damped zero, and the phase (Figure 2.6b) clearly indicates non-minimum phase behavior.

Such non-minimum phase zero when using load cells has also been observed on other mechanical systems [5–7]. It could be induced to small non-linearity in the system, but the reason of this non-minimum phase for the APA300ML is not yet clear.

However, this is not so important here as the zero is lightly damped (i.e. very close to the imaginary axis), and the closed loop poles (see the Root Locus plot in Figure 2.10b) should not be unstable except for very large controller gains that will never be applied in practice.

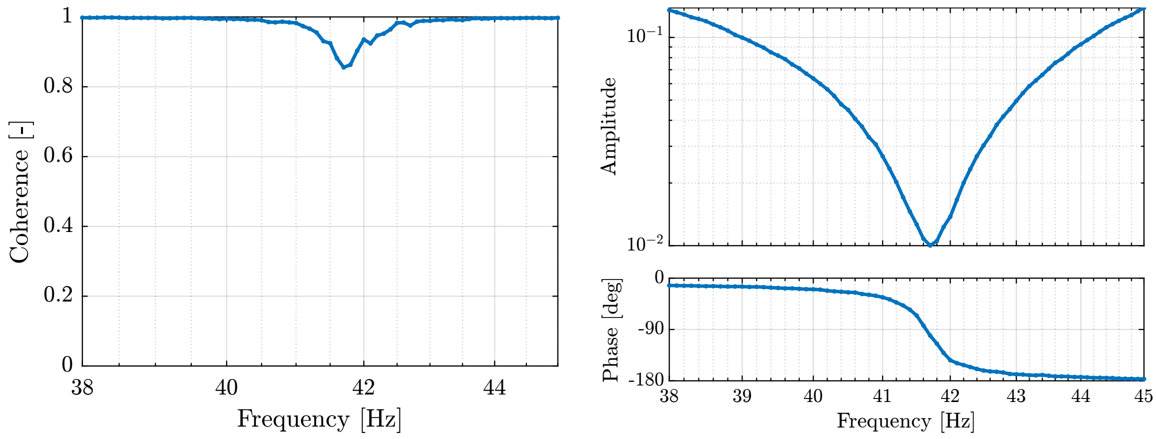

(a) Coherence

(b) Zoom on the non-minimum phase zero

Figure 2.6: Measurement of the anti-resonance found on the transfer function from u to V_s. The coherence (a) is quite good around the anti-resonance frequency. The phase (b) shoes a non-minimum phase behavior.

2.5 Effect of the resistor on the IFF Plant

A resistor $R \approx 80.6\,k\Omega$ is added in parallel with the sensor stack which has the effect to form a high pass filter with the capacitance of the piezoelectric stack (capacitance estimated at $\approx 5\,\mu F$).

As explain before, this is done to limit the voltage offset due to the input bias current of the ADC as well as to limit the low frequency gain.

The (low frequency) transfer function from u to V_s with and without this resistor have been measured and are compared in Figure 2.7. It is confirmed that the added resistor as the effect of adding an high pass filter with a cut-off frequency of $\approx 0.39\,\text{Hz}$.

2.6 Integral Force Feedback

In order to implement the Integral Force Feedback strategy, the measured frequency response function from u to V_s (Figure 2.5b) is fitted using the transfer function shown in equation (2.3). The parameters are manually tuned, and the obtained values are $\omega_{\text{HPF}} = 0.4\,\text{Hz}$, $\omega_z = 42.7\,\text{Hz}$, $\xi_z = 0.4\,\%$, $\omega_p = 95.2\,\text{Hz}$, $\xi_p = 2\,\%$ and $g_0 = 0.64$.

$$G_{\text{IFF},m}(s) = g_0 \cdot \frac{1 + 2\xi_z \frac{s}{\omega_z} + \frac{s^2}{\omega_z^2}}{1 + 2\xi_p \frac{s}{\omega_p} + \frac{s^2}{\omega_p^2}} \cdot \frac{s}{\omega_{\text{HPF}} + s} \tag{2.3}$$

The comparison between the identified plant and the manually tuned transfer function is done in Figure 2.8.

The implemented Integral Force Feedback Controller transfer function is shown in equation (2.4). It

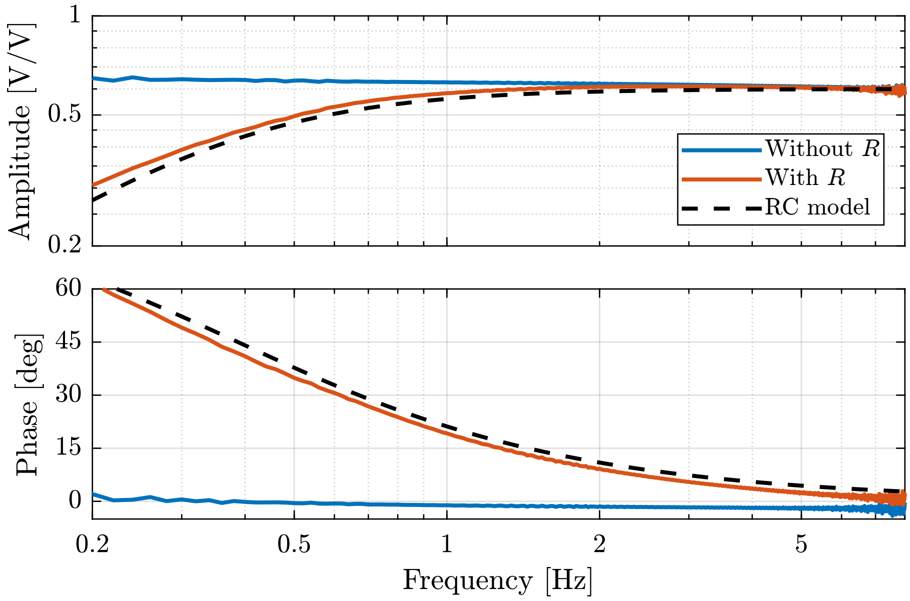

Figure 2.7: Transfer function from u to V_s with and without the resistor R in parallel with the piezoelectric stack used as the force sensor

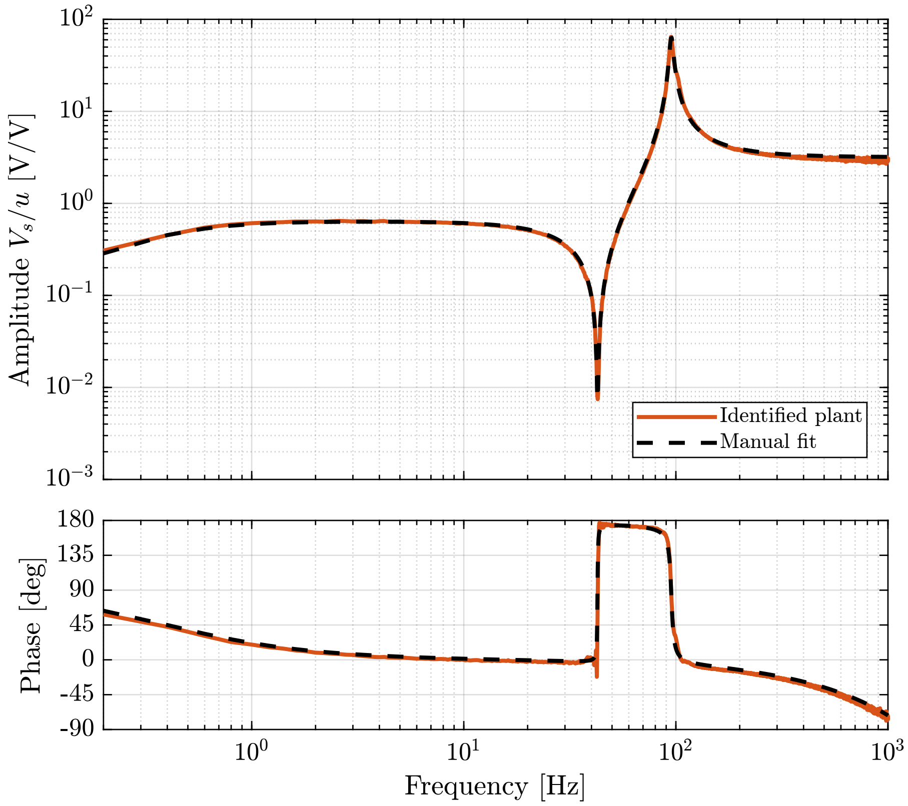

Figure 2.8: Identified IFF plant and manually tuned model of the plant (a time delay of $200\,\mu s$ is added to the model of the plant to better match the identified phase)

contains an high pass filter (cut-off frequency of 2 Hz) to limit the low frequency gain, a low pass filter to add integral action above 20 Hz, a second low pass filter to add robustness to high frequency resonances and a tunable gain g.

$$K_{\text{IFF}}(s) = -10 \cdot g \cdot \frac{s}{s + 2\pi \cdot 2} \cdot \frac{1}{1 + 2\pi \cdot 20} \cdot \frac{1}{s + 2\pi \cdot 2000} \tag{2.4}$$

To estimate how the dynamics of the APA changes when the Integral Force Feedback controller is implemented, the test bench shown in Figure 2.9 is used. The transfer function from the "damped" plant input $u\prime$ to the encoder displacement d_e is identified for several IFF controller gains g.

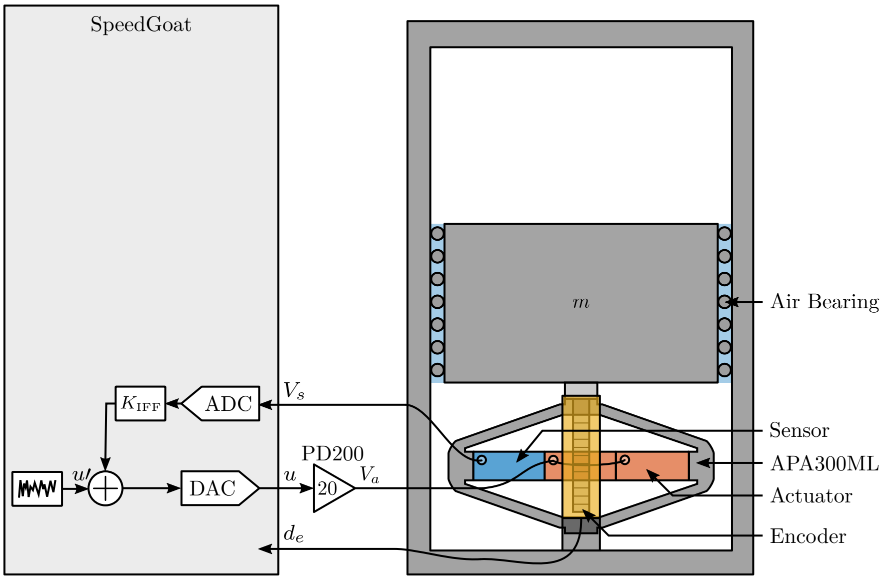

Figure 2.9: Implementation of Integral Force Feedback in the Speedgoat. The damped plant has a new input $u\prime$

The identified dynamics are then fitted by second order transfer functions[3]. The comparison between the identified damped dynamics and the fitted second order transfer functions is done in Figure 2.10a for different gains g. It is clear that large amount of damping is added when the gain is increased and that the frequency of the pole is shifted to lower frequencies.

The evolution of the pole in the complex plane as a function of the controller gain g (i.e. the "root locus") is computed both using the IFF plant model (2.3) and the implemented controller (2.4) and from the fitted transfer functions of the damped plants experimentally identified for several controller gains. The two obtained root loci are compared in Figure 2.10b and are in good agreement considering that the damped plants were only fitted using a second order transfer function.

[3]The transfer function fitting was computed using the `vectfit3` routine, see [8]

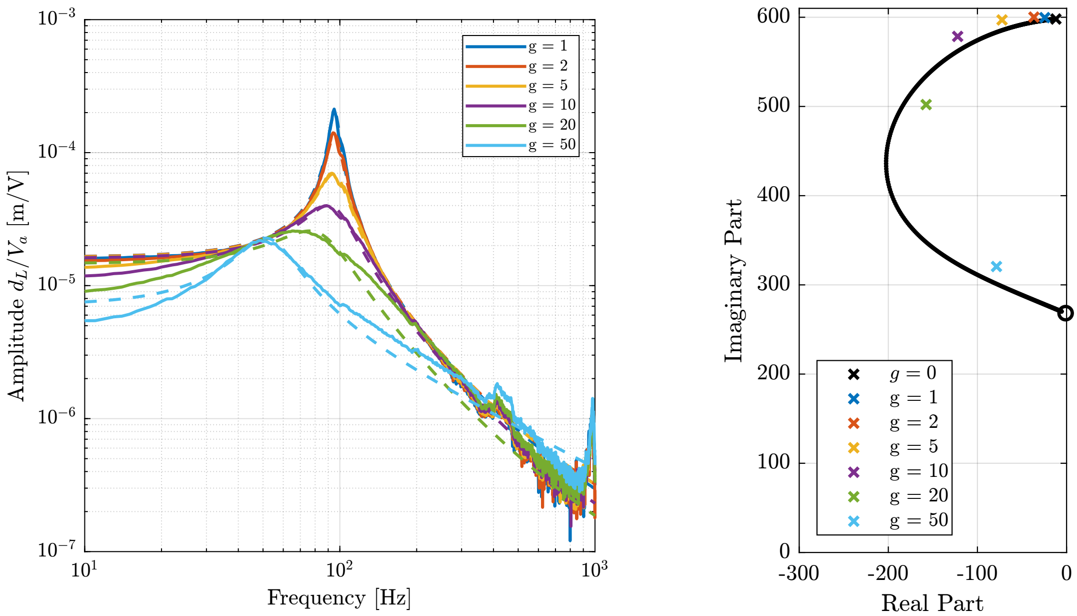

(a) Measured frequency response functions of damped plants for several IFF gains (solid lines). Identified 2nd order plants to match the experimental data (dashed lines)

(b) Root Locus plot using the plant model (black) and poles of the identified damped plants (color crosses)

Figure 2.10: Experimental results of applying Integral Force Feedback to the APA300ML. Obtained damped plant (a) and Root Locus (b)

3 APA300ML - 2 Degrees of Freedom Model

In this section, a simscape model (Figure 3.1) of the measurement bench is used to compare the model of the APA with the measured frequency response functions.

A 2 degrees of freedom model is used to model the APA300ML. This model is presented in Section 3.1 and the procedure to tuned the model is described in Section 3.2. The obtained model dynamics is compared with the measurements in Section 3.3.

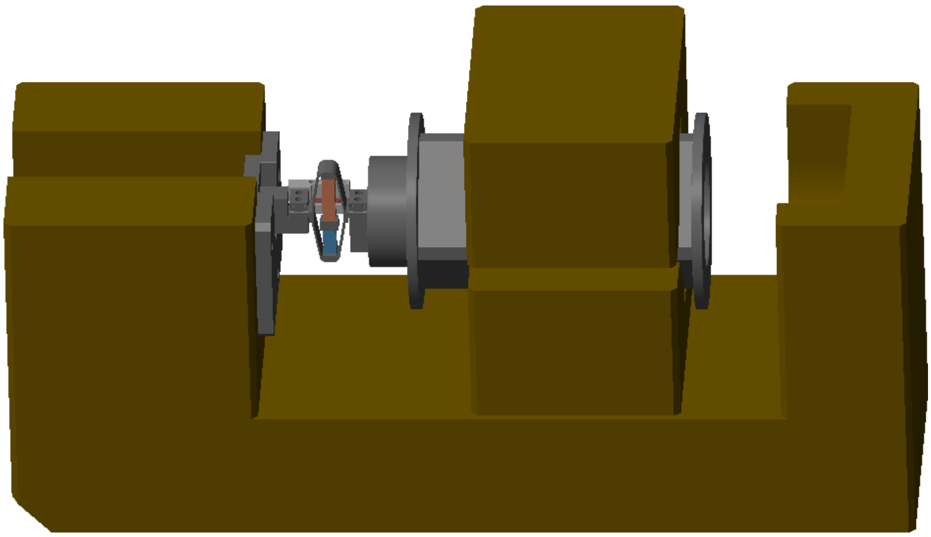

Figure 3.1: Screenshot of the Simscape model

3.1 Two Degrees of Freedom APA Model

The model of the amplified piezoelectric actuator is shown in Figure 3.2. It can be decomposed into three components:

- the shell whose axial properties are represented by k_1 and c_1
- the actuator stacks whose contribution in the axial stiffness is represented by k_a and c_a. A force source τ represents the axial force induced by the force sensor stacks. The gain g_a (in N/m) is used to convert the applied voltage V_a to the axial force τ

- the sensor stack whose contribution in the axial stiffness is represented by k_e and c_e. A sensor measures the stack strain d_L which is then converted to a voltage V_s using a gain g_s (in V/m)

Such simple model has some limitations:

- it only represents the axial characteristics of the APA as it is modelled as infinitely rigid in the other directions
- some physical insights are lost such as the amplification factor, the real stress and strain in the piezoelectric stacks
- it is fully linear and therefore the creep and hysteresis of the piezoelectric stacks are not modelled

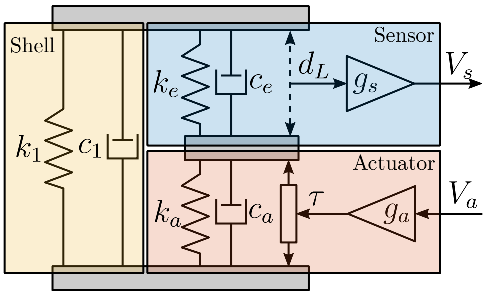

Figure 3.2: Schematic of the two degrees of freedom model of the APA300ML, adapted from [9]

3.2 Tuning of the APA model

9 parameters (m, k_1, c_1, k_e, c_e, k_a, c_a, g_s and g_a) have to be tuned such that the dynamics of the model (Figure 3.3) well represents the identified dynamics in Section 2.

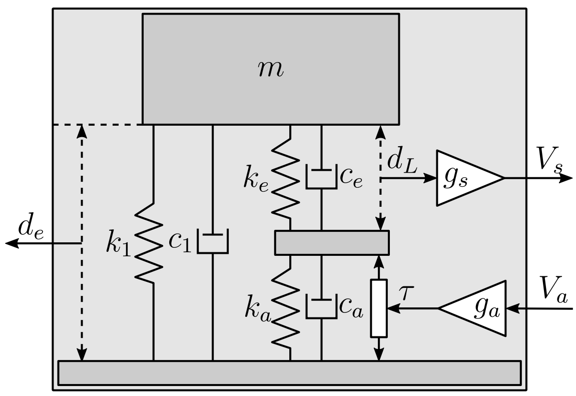

Figure 3.3: Schematic of the two degrees of freedom model of the APA300ML with input V_a and outputs d_e and V_s

First, the mass m supported by the APA300ML can be estimated from the geometry and density of the different parts or by directly measuring it using a precise weighing scale. Both methods leads to an estimated mass of $m = 5.7\,\text{kg}$.

Then, the axial stiffness of the shell was estimated at $k_1 = 0.38\,N/\mu m$ in Section 2.3 from the frequency of the anti-resonance seen on Figure 2.5b. Similarly, c_1 can be estimated from the damping ratio of the same anti-resonance and is found to be close to $20\,Ns/m$.

Then, it is reasonable to make the assumption that the sensor stacks and the two actuator stacks have identical mechanical characteristics[1]. Therefore, we have $k_e = 2k_a$ and $c_e = 2c_a$ as the actuator stack is composed of two stacks in series. In that case, the total stiffness of the APA model is described by (3.1).

$$k_{\text{tot}} = k_1 + \frac{k_e k_a}{k_e + k_a} = k_1 + \frac{2}{3}k_a \tag{3.1}$$

Knowing from (3.2) that the total stiffness is $k_{\text{tot}} = 2\,N/\mu m$, we get from (3.1) that $k_a = 2.5\,N/\mu m$ and $k_e = 5\,N/\mu m$.

$$\omega_0 = \frac{k_{\text{tot}}}{m} \Longrightarrow k_{\text{tot}} = m\omega_0^2 = 2\,N/\mu m \quad \text{with } m = 5.7\,\text{kg and } \omega_0 = 2\pi \cdot 95\,\text{rad}/s \tag{3.2}$$

Then, c_a (and therefore $c_e = 2c_a$) can be tuned to match the damping ratio of the identified resonance. $c_a = 100\,Ns/m$ and $c_e = 200\,Ns/m$ are obtained.

Finally, the two gains g_s and g_a can be tuned to match the gain of the identified transfer functions.

The obtained parameters of the model shown in Figure 3.3 are summarized in Table 3.1.

Parameter	**Value**
m	$5.7\,\text{kg}$
k_1	$0.38\,N/\mu m$
k_e	$5.0\,N/\mu m$
k_a	$2.5\,N/\mu m$
c_1	$20\,Ns/m$
c_e	$200\,Ns/m$
c_a	$100\,Ns/m$
g_a	$-2.58\,N/V$
g_s	$0.46\,V/\mu m$

Table 3.1: Summary of the obtained parameters for the 2 DoF APA300ML model

3.3 Obtained Dynamics

The dynamics of the two degrees of freedom model of the APA300ML is now extracted using optimized parameters (listed in Table 3.1) from the Simscape model. It is compared with the experimental data in Figure 3.4. A good match can be observed between the model and the experimental data, both for the encoder (Figure 3.4a) and for the force sensor (Figure 3.4b). This indicates that this model represents well the axial dynamics of the APA300ML.

[1] Note that this is not fully correct as it was shown in Section 2.2 that the electrical boundaries of the piezoelectric stack impacts its stiffness and that the sensor stack is almost open-circuited while the actuator stacks are almost short-circuited.

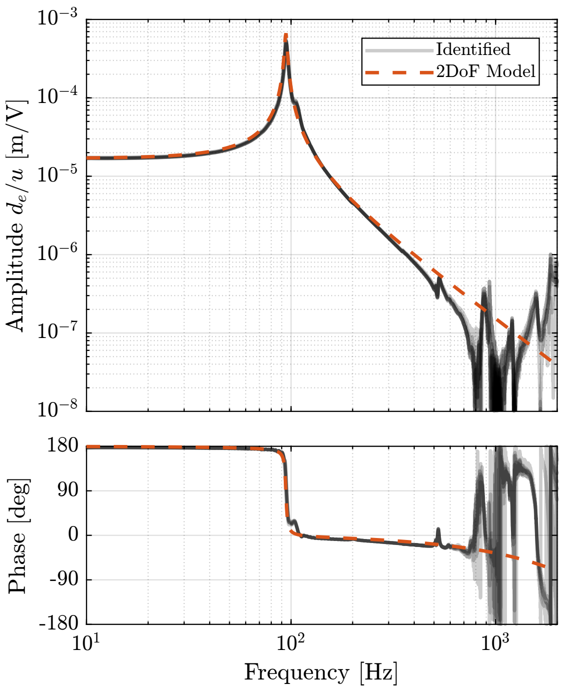

(a) from u to d_e

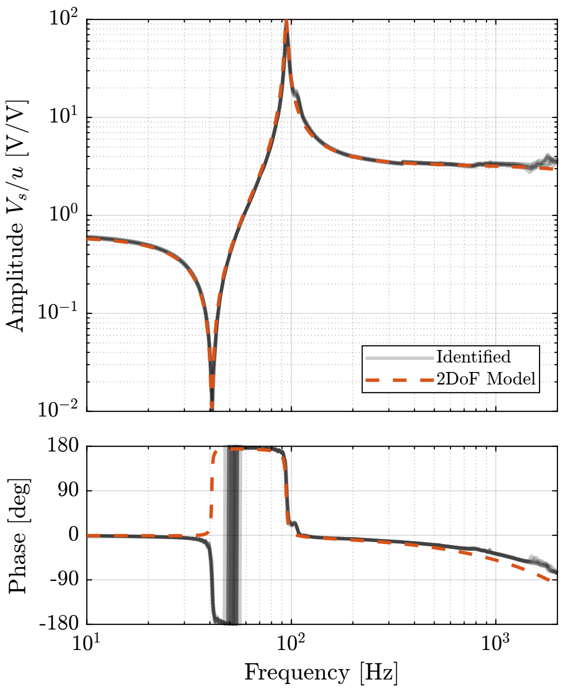

(b) from u to V_s

Figure 3.4: Comparison of the measured frequency response functions and the identified dynamics from the 2DoF model of the APA300ML. Both for the dynamics from u to d_e (a) (b) and from u to V_s (b)

4 APA300ML - Super Element

In this section, a *super element* of the APA300ML is computed using a finite element software[1]. It is then imported in Simscape (in the form of a stiffness matrix and a mass matrix) and included in the same model that was used in 3. This procedure is illustrated in Figure 4.1. Several *remote points* are defined in the finite element model (here illustrated by colorful planes and numbers from `1` to `5`) and are then make accessible in the Simscape model as shown at the right by the "frames" `F1` to `F5`.

For the APA300ML *super element*, 5 *remote points* are defined. Two *remote points* (`1` and `2`) are fixed to the top and bottom mechanical interfaces of the APA300ML and will be used for connecting the APA300ML with other mechanical elements. Two *remote points* (`3` and `4`) are located across two piezoelectric stacks and will be used to apply internal forces representing the actuator stacks. Finally, two *remote points* (`4` and `4`) are located across the third piezoelectric stack. It will be used to measure the strain experience by this stack, and model the sensor stack.

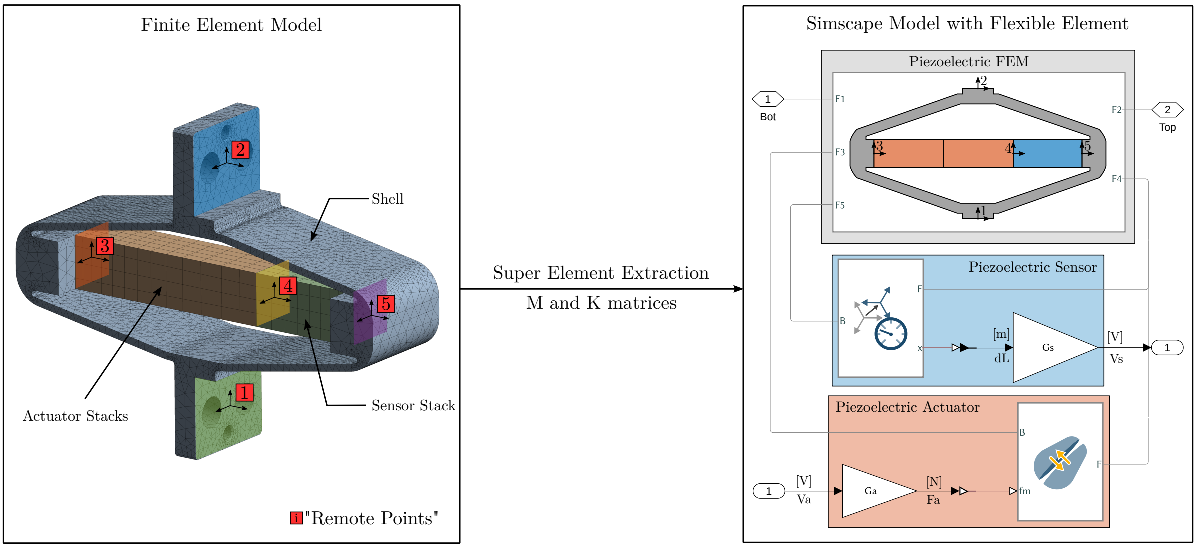

Figure 4.1: Finite Element Model of the APA300ML with "remotes points" on the left. Simscape model with included "Reduced Order Flexible Solid" on the right.

4.1 Identification of the Actuator and Sensor constants

Once the APA300ML *super element* is included in the Simscape model, the transfer function from F_a to d_L and d_e can be extracted. The gains g_a and g_s are then be tuned such that the gain of the transfer functions are matching the identified ones. By doing so, $g_s = 4.9\,V/\mu m$ and $g_a = 23.2\,N/V$ are obtained.

[1] Ansys® was used

To make sure these "gains" are physically valid, it is possible to estimate them from physical properties of the piezoelectric stack material.

From [2, p. 123], the relation between relative displacement d_L of the sensor stack and generated voltage V_s is given by (4.1a) and from [10] the relation between the force F_a and the applied voltage V_a is given by (4.1b).

$$V_s = \underbrace{\frac{d_{33}}{\epsilon^T s^D n}}_{g_s} d_L \tag{4.1a}$$

$$F_a = \underbrace{d_{33} n k_a}_{g_a} \cdot V_a, \quad k_a = \frac{c^E A}{L} \tag{4.1b}$$

Unfortunately, the manufacturer of the stack was not willing to share the piezoelectric material properties of the stack used in the APA300ML. However, based on available properties of the APA300ML stacks in the data-sheet, the soft Lead Zirconate Titanate "THP5H" from Thorlabs seemed to match quite well the observed properties. The properties of this "THP5H" material used to compute g_a and g_s are listed in Table 4.1.

From these parameters, $g_s = 5.1\,V/\mu m$ and $g_a = 26\,N/V$ were obtained which are close to the identified constants using the experimentally identified transfer functions.

Parameter	**Value**	**Description**
d_{33}	$680 \cdot 10^{-12}\,m/V$	Piezoelectric constant
ϵ^T	$4.0 \cdot 10^{-8}\,F/m$	Permittivity under constant stress
s^D	$21 \cdot 10^{-12}\,m^2/N$	Elastic compliance understand constant electric displacement
c^E	$48 \cdot 10^9\,N/m^2$	Young's modulus of elasticity
L	$20\,mm$ per stack	Length of the stack
A	$10^{-4}\,m^2$	Area of the piezoelectric stack
n	160 per stack	Number of layers in the piezoelectric stack

Table 4.1: Piezoelectric properties used for the estimation of the sensor and actuators "gains"

4.2 Comparison of the obtained dynamics

The obtained dynamics using the *super element* with the tuned "sensor gain" and "actuator gain" are compared with the experimentally identified frequency response functions in Figure 4.2. A good match between the model and the experimental results is observed. It is however a bit surprising that the model is a bit "softer" than the measured system as finite element models are usually overestimating the stiffness.

Using this simple test bench, it can be concluded that the *super element* model of the APA300ML well captures the axial dynamics of the actuator (the actuator stacks, the force sensor stack as well as the shell used as a mechanical lever).

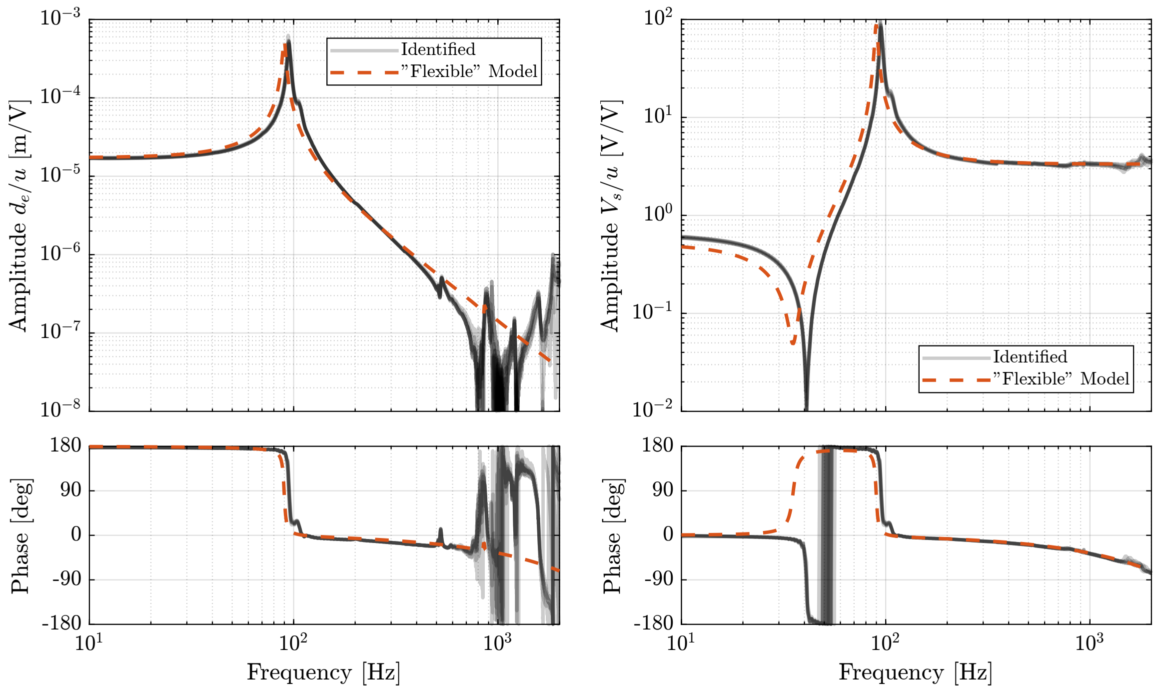

(a) from u to d_e

(b) from u to V_s

Figure 4.2: Comparison of the measured frequency response functions and the identified dynamics from the "flexible" model of the APA300ML. Both for the dynamics from u to d_e (a) (b) and from u to V_s (b)

5 Conclusion

The main characteristics of the APA300ML such as hysteresis and axial stiffness have been measured and were found to comply with the specifications.

The dynamics of the received APA were measured and found to all be identical (Figure 2.5). Even tough a non-minimum zero was observed on the transfer function from u to V_s (Figure 2.6), it was not found to be problematic as large amount of damping could be added using the integral force feedback strategy (Figure 2.10).

- Compare 2DoF and FEM models (usefulness of the two)
- Good match between all the APA: will simplify the modeling and control of the nano-hexapod
- No advantage of the FEM model here (as only uniaxial behavior is checked), but may be useful later

Bibliography

[1] E. Wehrsdorfer, G. Borchhardt, W. Karthe, and G. Helke, "Large signal measurements on piezoelectric stacks," *Ferroelectrics*, vol. 174, no. 1, pp. 259–275, 1995 (cit. on p. 5).

[2] A. J. Fleming and K. K. Leang, *Design, Modeling and Control of Nanopositioning Systems* (Advances in Industrial Control). Springer International Publishing, 2014 (cit. on pp. 10, 24).

[3] M. Reza and F. Andrew, *Piezoelectric Transducers for Vibration Control and Damping*. London: Springer, 2006 (cit. on p. 12).

[4] A. Preumont, *Vibration Control of Active Structures - Fourth Edition* (Solid Mechanics and Its Applications). Springer International Publishing, 2018 (cit. on p. 12).

[5] J. Spanos, Z. Rahman, and G. Blackwood, "A soft 6-axis active vibration isolator," in *Proceedings of 1995 American Control Conference - ACC'95*, 1995 (cit. on p. 13).

[6] D. Thayer, M. Campbell, J. Vagners, and A. von Flotow, "Six-axis vibration isolation system using soft actuators and multiple sensors," *Journal of Spacecraft and Rockets*, vol. 39, no. 2, pp. 206–212, 2002 (cit. on p. 13).

[7] G. Hauge and M. Campbell, "Sensors and control of a space-based six-axis vibration isolation system," *Journal of Sound and Vibration*, vol. 269, no. 3-5, pp. 913–931, 2004 (cit. on p. 13).

[8] A. Gustavsen B.; Semlyen, "Rational approximation of frequency domain responses by vector fitting," *IEEE Transactions on Power Delivery*, vol. 14, 3 Jul. 1999 (cit. on p. 16).

[9] A. Souleille, T. Lampert, V. Lafarga, *et al.*, "A concept of active mount for space applications," *CEAS Space Journal*, vol. 10, no. 2, pp. 157–165, 2018 (cit. on p. 18).

[10] A. J. Fleming and K. K. Leang, "Integrated strain and force feedback for high-performance control of piezoelectric actuators," *Sensors and Actuators A: Physical*, vol. 161, no. 1-2, pp. 256–265, 2010 (cit. on p. 24).